

## Average angular momentum in fusion reactions deduced from evaporation-residue cross sections

O. A. Capurro and D. E. DiGregorio

Laboratorio TANDAR, Departamento de Física, Comisión Nacional de Energía Atómica, Av. del Libertador 8250,  
1429 Buenos Aires, Argentina

(Received 9 September 1997)

Average angular momenta of compound nuclei were deduced from measured evaporation-residue cross sections on the basis of statistical model calculations. We have applied this method to the following systems:  $^4\text{He} + ^{197}\text{Au}$ ,  $^{16}\text{O} + ^{147,149,152,154}\text{Sm}$ ,  $^{32}\text{S} + ^{138}\text{Ba}$ , and  $^{48}\text{Ti} + ^{122}\text{Sn}$ . For some of these systems, the average angular momenta were compared with those extracted from early  $\gamma$ -multiplicity measurements. A reasonable agreement was found between the values of the deduced average angular momentum obtained from both methods, giving support to the validity of the present method. The average angular momenta for all the systems exhibit the energy dependence predicted by a standard fusion model calculation. [S0556-2813(98)01501-5]

PACS number(s): 25.70.Gh

Knowledge of the first moment of the angular momentum distribution acts as a constraint for fusion models. Consequently, a more stringent test of the theoretical models can be obtained by comparing their predictions with the experimental average angular momentum of the compound nucleus. In this work, we have analyzed the experimental yields for the evaporation residues produced in fusion reactions to deduce the average angular momentum of the compound nucleus. The relationship between the measured relative cross sections for the evaporation residues and the average angular momentum of the compound nucleus was established through statistical model calculations. We have applied this method as a natural extension of the studies on isomer ratios reported in previous publications [1,2]. This technique has been employed for some reactions that form compound nuclei of mass number  $A \sim 100$  [3].

The procedure carried out in the present analysis is completely analogous to that followed and described for the isomer ratios in Ref. [2]. For the present case, we define the ratio between the yields for the  $(x+1)m$  and  $xm$  evaporation-residue channels ( $m$  indicates neutrons and/or protons) as

$$\frac{Y_{(x+1)m}}{Y_{xm}} = \frac{\sigma_{(x+1)m}/\sigma_{\text{fus}}}{\sigma_{xm}/\sigma_{\text{fus}}} = \frac{\sum_J \sigma_J Y_{J,(x+1)m}}{\sum_J \sigma_J Y_{J,xm}}, \quad (1)$$

where  $\sigma_{(x+1)m}$  and  $\sigma_{xm}$  are the cross sections for the evaporation of  $(x+1)$  and  $x$  nucleons,  $\sigma_{\text{fus}}$  is the fusion cross section,  $\sigma_J$  is the cross section for the formation of the compound nucleus with total angular momentum  $J$ , and  $Y_{J,(x+1)m}$  and  $Y_{J,xm}$  are the relative yields for the  $(x+1)m$  and  $xm$  evaporated nucleons for the compound nucleus at fixed excitation energy and total angular momentum  $J$ .

The cross section for the formation of the compound nucleus,  $\sigma_J$ , taking into account the values of intrinsic spins of the reactants,  $s_1$  and  $s_2$ , can be expressed in terms of the partial angular momentum distributions  $\sigma_l$ ,

$$\sigma_J = \frac{(2J+1)}{(2s_1+1)(2s_2+1)} \sum_{s=|s_1-s_2|}^{s_1+s_2} \sum_{l=|J-s|}^{J+s} \frac{\sigma_l}{2l+1}, \quad (2)$$

where  $\vec{J} = \vec{l} + \vec{S}$  and  $\vec{S} = \vec{s}_1 + \vec{s}_2$ . The average angular momentum  $\langle J \rangle$  of the compound nucleus can be evaluated as

$$\langle J \rangle = \frac{\sum_J J \sigma_J}{\sum_J \sigma_J}, \quad (3)$$

There is no difference between the values of  $\langle J \rangle$  and  $\langle l \rangle$  (defined as  $\langle l \rangle = \sum_l l \sigma_l / \sum_l \sigma_l$ ) when the intrinsic spins of the projectile and the target are equal to zero.

Equations (1) and (3) establish the connection between the relative yields and the average angular momentum which has to be quantitatively determined through statistical model calculations and the comparison of the experimental and calculated values of  $Y_{(x+1)m}/Y_{xm}$ . We chose the Monte Carlo code PACE [4] to simulate the Hauser-Feshbach compound nucleus decay mode. The first step in the analysis was to adopt a set of input parameters for the statistical model calculations. This was done by fitting the experimental ratios ( $Y_{(x+1)m}/Y_{xm}$ ) at energies well above the Coulomb barrier where the spin distribution  $\sigma_J$  has a known triangular shape for every fusion model. Then, a series of statistical model calculations were performed to obtain  $Y_{J,(x+1)m}$  and  $Y_{J,xm}$  at different excitation energies. Knowledge of these calculated relative yields enables us to determine the theoretical ratio  $Y_{(x+1)m}/Y_{xm}$  for any initial angular momentum distribution. Finally, we searched for the angular momentum distribution whose theoretical ratio  $Y_{(x+1)m}/Y_{xm}$  agrees with the corresponding experimental value. To ensure a general survey of all typical shapes of angular momentum distribution,

$$\sigma_l = \frac{\pi}{k^2} (2l+1) T_l, \quad (4)$$

the transmission coefficient  $T_l$  was parametrized assuming a Fermi function,

$$T_l = \frac{1}{1 + \exp[(l-l_0)/\Delta l]}, \quad (5)$$

where both  $l_0$  and  $\Delta l$  were considered as free parameters. In this manner, a wide family of distributions with different shapes (from bell-like to triangular shapes) was obtained as

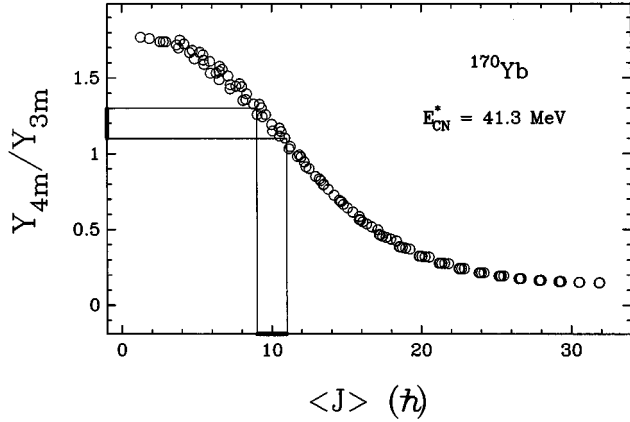


FIG. 1. Relation between the ratio  $Y_{4m}/Y_{3m}$  and the average angular momentum for the compound nucleus  $^{170}\text{Yb}$  at  $E_{\text{CN}}^* = 41.3$  MeV. Statistical model calculations were performed to obtain  $Y_{J,4m}$  and  $Y_{J,3m}$  for every  $J$  at this excitation energy. These calculated relative yields enables to determine the ratio  $Y_{4m}/Y_{3m}$  for any initial angular momentum distribution applying Eq. (1). A Fermi function was used for the shape of the transmission coefficient whose parameters  $l_0$  and  $\Delta l$  were varied to obtain a wide family of spin distributions. These spin distributions span from bell-like shape (small  $l_0$  and large  $\Delta l$ ) to triangular shape (large  $l_0$  and small  $\Delta l$ ). Their average angular momenta were obtained from Eq. (3).

done in Ref. [2]. In Eq. (4),  $k$  is the wave number associated with the center-of-mass bombarding energy.

In order to investigate the ability of the method described above, we performed the following statistical model calculations for the  $^{16}\text{O} + ^{152}\text{Sm}$  and  $^{16}\text{O} + ^{154}\text{Sm}$  systems.

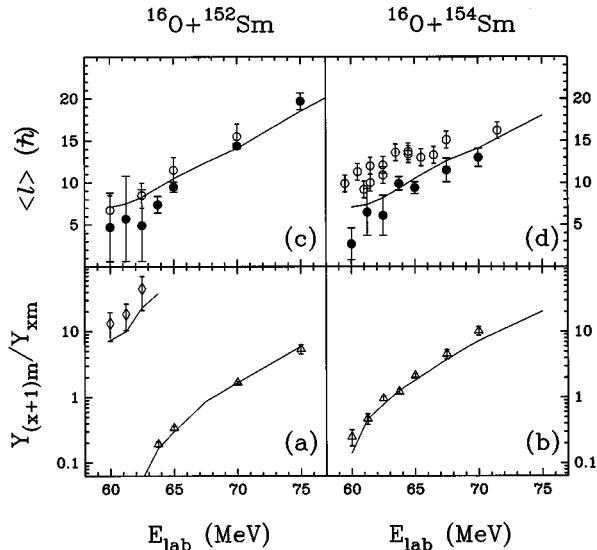


FIG. 2. (a) and (b) Experimental ratios  $Y_{(x+1)m}/Y_{xm}$  for the  $^{16}\text{O} + ^{152}\text{Sm}$  and  $^{16}\text{O} + ^{154}\text{Sm}$  systems (open diamonds for  $x=2$  and open triangles for  $x=3$ ). These data were reported in Ref. [5]. The solid lines are the results of the combined calculations of codes CCDEF and PACE (see text for details). (c) and (d) The average angular momentum deduced from the experimental ratios  $Y_{(x+1)m}/Y_{xm}$  is plotted for both systems (solid circles). The open circles are the  $\langle l \rangle$  values deduced from  $\gamma$ -multiplicity measurements [10,11]. The solid lines correspond to the mean value of the  $l$  distributions estimated by CCDEF.

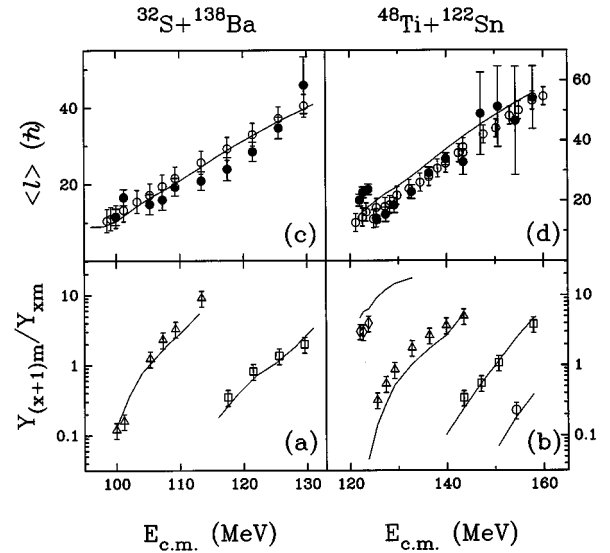


FIG. 3. (a) and (b) Experimental ratios  $Y_{(x+1)m}/Y_{xm}$  for the  $^{32}\text{S} + ^{138}\text{Ba}$  and  $^{48}\text{Ti} + ^{122}\text{Sn}$  systems (open diamonds, triangles, squares, and circles for  $x=2, 3, 4$ , and  $5$ , respectively). These data were reported in Ref. [6]. We adopted a 25% as total error for all ratios in these systems (the authors only report statistical errors of the fusion cross sections). The solid lines are the results of the combined calculations of codes CCDEF and PACE (see text for details). (c) and (d) The average angular momentum deduced from the experimental ratios  $Y_{(x+1)m}/Y_{xm}$  is plotted for both systems (solid circles). The percentual errors of the deduced  $\langle l \rangle$  values are significantly larger than the corresponding residue ratios at the highest energies in the  $^{48}\text{Ti} + ^{122}\text{Sn}$  system. This occurs because the ratio  $Y_{5m}/Y_{4m}$  reaches the saturation region (see Fig. 1) since the fission channel begins to compete with the  $4m$  channel for large  $J_{\text{CN}}$  values. The open circles are the  $\langle l \rangle$  values deduced from  $\gamma$ -multiplicity measurements [12]. The solid lines correspond to the mean value of the  $l$  distributions estimated by CCDEF.

tions for the  $^{16}\text{O} + ^{154}\text{Sm}$  system. The fusion of these nuclei leads to the formation of compound nucleus  $^{170}\text{Yb}$ . At the laboratory bombarding energy of 63.8 MeV, the excitation energy of this compound nucleus is 41.3 MeV. We calculated the ratio  $Y_{4m}/Y_{3m}$  and  $\langle J \rangle$  according to Eqs. (1) and (3), respectively. We used Fermi angular momentum distributions with  $l_0$  varying from  $2\hbar$  to  $56\hbar$  in steps of  $2\hbar$ , and  $\Delta l$  from  $0.2\hbar$  to  $2.7\hbar$  in steps of  $0.5\hbar$ . The results of these calculations are shown in Fig. 1. The correlation between the ratio  $Y_{4m}/Y_{3m}$  and  $\langle J \rangle$  is represented by open circles. As can be seen in this figure, there is practically a one-to-one correspondence between the ratio and the average angular momentum. In other words, different  $l$  distributions having similar average values lead to similar evaporation-residue ratios. For example, a ratio of  $1.2 \pm 0.1$  leads to a  $\langle J \rangle$  value of  $(10 \pm 1)\hbar$ . However, it must be noted that there is a region where the correlation is not single valued. This happens for large  $\langle J \rangle$  values because the highest partial waves of these distributions only contribute to feed the  $Y_{2m}$  yield. In any case, this is not a problem since the deduction of  $\langle J \rangle$  was always carried out through the ratio between the two dominant evaporation-residue yields at each energy. In summary, Fig. 1 substantiates the validity of the technique to deduce

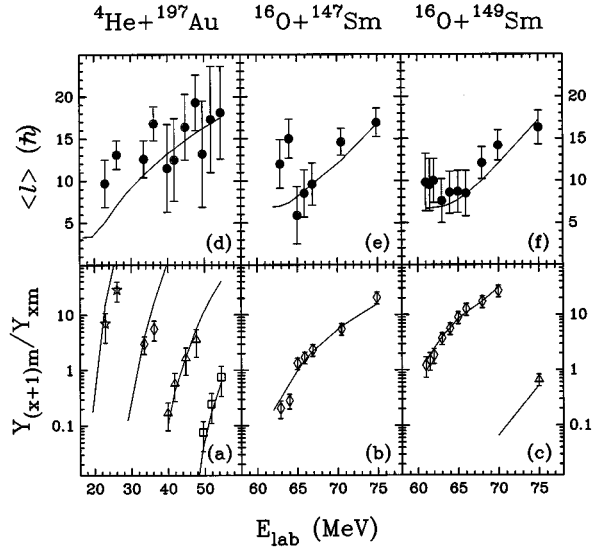


FIG. 4. (a), (b), and (c) Experimental ratios  $Y_{(x+1)m}/Y_{xm}$  for the  ${}^4\text{He}+{}^{197}\text{Au}$ ,  ${}^{16}\text{O}+{}^{147}\text{Sm}$ , and  ${}^{16}\text{O}+{}^{149}\text{Sm}$  systems (open stars, diamonds, triangles, and squares for  $x=1, 2, 3$ , and  $4$ , respectively). These data are reported in Refs. [7] (for the first system) and [8] (for the other systems). The solid lines are the results of the combined calculations of codes CCDEF and PACE (see text for details). (d), (e), and (f) The average angular momentum deduced from the experimental ratios  $Y_{(x+1)m}/Y_{xm}$  is plotted for these systems (solid circles). The solid lines correspond to the mean value of the  $l$  distributions estimated by CCDEF.

the average value of the initial spin distribution by measuring the ratio of the evaporation-residue cross sections of the two dominant decay modes for the fusion-evaporation process.

Using the present method, we deduced the average angular momentum for some systems:  ${}^{16}\text{O}+{}^{152,154}\text{Sm}$ ,  ${}^{32}\text{S}+{}^{138}\text{Ba}$ ,  ${}^{48}\text{Ti}+{}^{122}\text{Sn}$ ,  ${}^4\text{He}+{}^{197}\text{Au}$ , and  ${}^{16}\text{O}+{}^{147,149}\text{Sm}$ . The evaporation-residue cross sections were reported in Refs. [5–8]. The experimental ratios  $Y_{(x+1)m}/Y_{xm}$  are plotted as a function of the bombarding energy in Figs. 2(a), 2(b), 3(a), 3(b), 4(a), 4(b), and 4(c), and are indicated with open stars, diamonds, triangles, squares, and circles for  $x = 1, 2, 3, 4$ ,

and 5, respectively. The solid lines represent the results of the statistical model calculation performed by the code PACE using as input the angular momentum distribution predicted by the fusion model code CCDEF [9]. In this code we adjusted the depth of the nuclear potential to fix the Coulomb barrier parameters for every system considered here. For those systems involving samarium isotopes as target nuclei, we included the coupling to the quadrupole deformation of the target in the CCDEF calculation. Besides this deformation, the coupling to inelastic and transfer channels was included in the calculations for  ${}^{32}\text{S}+{}^{138}\text{Ba}$  and  ${}^{48}\text{Ti}+{}^{122}\text{Sn}$  according to Ref. [6]. No coupling was considered in the CCDEF calculation for  ${}^4\text{He}+{}^{197}\text{Au}$ . The values of the input parameters used in the code PACE for each system are presented in Table I. Wherever possible we adopted the same input parameters determined from analyses of previous studies [5,6,8]. The remaining input parameters, such as the optical-model parameters for the transmission coefficients, were as described in Ref. [4]. We can observe a very good agreement between calculated and experimental fractional evaporation-residue yields for all the systems, with a few exceptions at the lowest bombarding energies.

Figures 2(c), 2(d), 3(c), 3(d), 4(d), 4(e), and 4(f) display the deduced  $\langle l \rangle$  values as a function of the bombarding energy for all systems studied in the present work (solid circles). The deduced  $\langle l \rangle$  values, obtained from  $\gamma$ -multiplicity measurements for  ${}^{16}\text{O}+{}^{152}\text{Sm}$  [10],  ${}^{16}\text{O}+{}^{154}\text{Sm}$  [11],  ${}^{32}\text{S}+{}^{138}\text{Ba}$  [12], and  ${}^{48}\text{Ti}+{}^{122}\text{Sn}$  [12], are also shown (open circles). The solid lines correspond to the predicted average angular momentum by CCDEF. Our deduced  $\langle l \rangle$  values agree fairly well with the fusion model predictions as well as those values obtained through the  $\gamma$ -multiplicity technique.

In summary, the ratio of the evaporation-residue yields can become a useful tool to derive the average value of the initial spin distribution of the compound nucleus. This work is an extension of the analyses published for the isomer ratios in Ref. [2]. To achieve the purpose it is necessary to fit the experimental residue ratios over the whole energy range. In particular, this fitting must be very good at energies above the Coulomb barrier where the spin distribution is almost fusion-model independent. The proposed procedure for determining the average angular momentum in fusion reactions

TABLE I. Parameters used in the code PACE.

System	${}^{16}\text{O}+{}^{152,154}\text{Sm}$ (Ref. [5])	${}^{32}\text{S}+{}^{138}\text{Ba}$ ${}^{48}\text{Ti}+{}^{122}\text{Sn}$ (Ref. [6])	${}^4\text{He}+{}^{197}\text{Au}$	${}^{16}\text{O}+{}^{147}\text{Sm}$ (Ref. [8])	${}^{16}\text{O}+{}^{149}\text{Sm}$ (Ref. [8])
$a$ (MeV $^{-1}$ )	$A/8.5$	$A/9.0$	$A/11.5$	$A/8.5$	$A/8.5$
Yrast line	Sierk <sup>a</sup>	Sierk <sup>b</sup>	Gilbert-Cameron <sup>c</sup>	Sierk <sup>a</sup>	Sierk <sup>d</sup>
$E1$ (W.u.)	0.025	1.4 <sup>e</sup>	0.00001	0.025	0.025
$M1$ (W.u.)	0.01	0.01	0.01	0.01	0.01
$E2$ (W.u.)	9	9	9	9	9
$M2$ (W.u.)	1.2	1.2	1.2	1.2	1.2

<sup>a</sup>The rotational energies are obtained from Ref. [13].

<sup>b</sup>The rotational energies obtained from Ref. [13] are multiplied by a factor of 0.8.

<sup>c</sup>The rotational energies are obtained from Ref. [14].

<sup>d</sup>The rotational energies obtained from Ref. [13] are multiplied by a factor of 1.2.

<sup>e</sup>Fraction of sum rule exhausted by the integrated  $E1$  strength.

relies only on the statistical model parameters. The discrepancies observed at subbarrier energies for some of the systems studied in this paper can be originated in the fusion-model calculation and/or perhaps in the data due to the small cross sections involved.

We thank Dr. A.O. Gattone and Dr. A.J. Pacheco for the careful reading of this manuscript and their helpful suggestions. One of us (D.E.D.G.) acknowledges financial support from the Consejo Nacional de Investigaciones Científicas y Técnicas, Argentina.

- 
- [1] D.E. DiGregorio, K.T. Lesko, B.A. Harmon, E.B. Norman, J. Pouliot, B. Sur, Y. Chan, and R.G. Stokstad, *Phys. Rev. C* **42**, 2108 (1990).
- [2] O.A. Capurro, D.E. DiGregorio, S. Gil, D. Abriola, M. di Tada, J.O. Fernández Niello, A.O. Macchiavelli, G.V. Martí, A.J. Pacheco, J.E. Testoni, D. Tomasi, and I. Urteaga, *Phys. Rev. C* **55**, 766 (1997).
- [3] M. Dasgupta, A. Navin, Y.K. Agarwal, C.V.K. Baba, H.C. Jain, M.L. Jhingan, and A. Roy, *Phys. Rev. Lett.* **66**, 1414 (1991); *Pramana* **38**, 291 (1992).
- [4] A. Gavron, *Phys. Rev. C* **21**, 230 (1980).
- [5] R.G. Stokstad, Y. Eisen, S. Kaplanis, D. Pelte, U. Smilansky, and I. Tserruya, *Phys. Rev. C* **21**, 2427 (1980).
- [6] S. Gil, F. Hasenbalg, J.E. Testoni, D. Abriola, M.C. Berisso, M. di Tada, A. Etchegoyen, J.O. Fernández Niello, A.J. Pacheco, A.W. Charlop, A. Sonzogni, and R. Vandenbosch, *Phys. Rev. C* **51**, 1336 (1995).
- [7] O.A. Capurro, M. de la Vega Vedoya, C. Wasilevsky, and S.J. Nassiff, *J. Radioanalyt. Nucl. Chem., Articles* **89**, 519 (1987).
- [8] D.E. DiGregorio, M. di Tada, D. Abriola, M. Elgue, A. Etchegoyen, M.C. Etchegoyen, J.O. Fernández Niello, A. Ferrero, S. Gil, A.O. Macchiavelli, A.J. Pacheco, J.E. Testoni, P.R.S. Gomes, V. Vanin, R. Liguori Neto, E. Crema, and R. G. Stokstad, *Phys. Rev. C* **39**, 516 (1989).
- [9] J.O. Fernández Niello, C.H. Dasso, and S. Landowne, *Comput. Phys. Commun.* **54**, 409 (1989).
- [10] A.H. Wuosmaa, R.R. Betts, B.B. Back, M.P. Carpenter, H. Esbensen, P.B. Fernandez, B.G. Glagola, Th. Happ, R.V.F. Janssens, T.L. Khoo, E.F. Moore, F. Scarlassara, and Ph. Benet, *Phys. Lett. B* **263**, 23 (1991).
- [11] S. Gil, A.W. Charlop, A. Garcia, D.D. Leach, S.J. Luke, S. Kailas, and R. Vandenbosch, *Phys. Rev. C* **43**, 701 (1991).
- [12] A.W. Charlop, J.D. Bierman, Z. Drebi, S. Gil, D.J. Prindle, A. Sonzogni, R. Vandenbosch, and D. Ye, *Phys. Rev. C* **51**, 628 (1995).
- [13] A. Sierk, *Phys. Rev. C* **33**, 2039 (1986).
- [14] A. Gilbert and A.G.W. Cameron, *Can. J. Phys.* **43**, 1446 (1965).